Theoretical basis for interpreting heterodyne chirality-selective sum frequency generation spectra of water \odot

Special Collection: Recent Developments in Nonlinear Optics at Interfaces

Daniel Konstantinovsky [®] ; Ty Santiago [®] ; Matthew Tremblay [®] ; Garth J. Simpson [®] ; Sharon Hammes-Schiffer [™] [®] ; Elsa C. Y. Yan [™] [®]

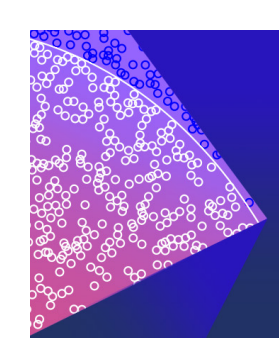


J. Chem. Phys. 160, 055102 (2024) https://doi.org/10.1063/5.0181718





CrossMark



The Journal of Chemical Physics

Special Topic: Monte Carlo methods, 70 years after Metropolis et al. (1953)

Submit Today





Theoretical basis for interpreting heterodyne chirality-selective sum frequency generation spectra of water

Cite as: J. Chem. Phys. 160, 055102 (2024); doi: 10.1063/5.0181718 Submitted: 17 October 2023 • Accepted: 8 January 2024 •

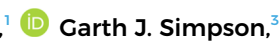






Published Online: 5 February 2024

Daniel Konstantinovsky, 1,2,a) Daniel Konstantinovsky, 1,2,a) Ty Santiago, 1 Daniel Konstantinovsky, 1,2,a) Garth J. Simpson, 3 Daniel Konstantinovsky, 1,2,a) Sharon Hammes-Schiffer. 1,4,b) and Elsa C. Y. Yan 1,b)







AFFILIATIONS

- Department of Chemistry, Yale University, New Haven, Connecticut 06520, USA
- ²Department of Molecular Biophysics and Biochemistry, Yale University, New Haven, Connecticut 06520, USA
- ³Department of Chemistry, Purdue University, West Lafayette, Indiana 47907, USA
- Department of Chemistry, Princeton University, Princeton, New Jersey 08544, USA

Note: This paper is part of the JCP Special Topic on Recent Developments in Nonlinear Optics at Interfaces.

- ^{a)}Current address: Department of Chemistry, Columbia University, New York, New York 10027, USA.
- b) Authors to whom correspondence should be addressed: shs566@princeton.edu and elsa.yan@yale.edu

ABSTRACT

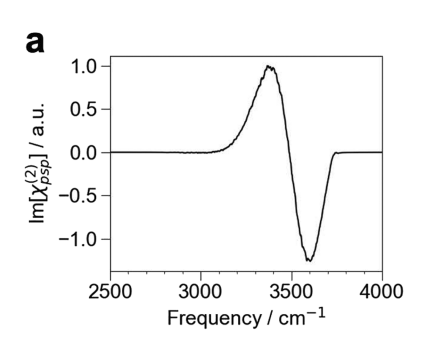
Chirality-selective vibrational sum frequency generation (chiral SFG) spectroscopy has emerged as a powerful technique for the study of biomolecular hydration water due to its sensitivity to the induced chirality of the first hydration shell. Thus far, water O-H vibrational bands in phase-resolved heterodyne chiral SFG spectra have been fit using one Lorentzian function per vibrational band, and the resulting fit has been used to infer the underlying frequency distribution. Here, we show that this approach may not correctly reveal the structure and dynamics of hydration water. Our analysis illustrates that the chiral SFG responses of symmetric and asymmetric O-H stretch modes of water have opposite phase and equal magnitude and are separated in energy by intramolecular vibrational coupling and a heterogeneous environment. The sum of the symmetric and asymmetric responses implies that an O-H stretch in a heterodyne chiral SFG spectrum should appear as two peaks with opposite phase and equal amplitude. Using pairs of Lorentzian functions to fit water O-H stretch vibrational bands, we improve spectral fitting of previously acquired experimental spectra of model β-sheet proteins and reduce the number of free parameters. The fitting allows us to estimate the vibrational frequency distribution and thus reveals the molecular interactions of water in hydration shells of biomolecules directly from chiral SFG spectra.

Published under an exclusive license by AIP Publishing. https://doi.org/10.1063/5.0181718

INTRODUCTION

Spectral fitting has been a standard approach for extracting molecular information from vibrational spectra, including those obtained by chirality-sensitive vibrational sum frequency generation (chiral SFG) spectroscopy. In recent years, chiral SFG has emerged as a powerful technique for studying the macromolecular hydration shell. 1-6 Few experimental techniques are able to probe water in biological hydration shells selectively. As a surface-selective technique, chiral SFG is able to resolve chirality at interfaces. 4,7-13 Our group has shown that this technique is selective to the first hydration shell around a β-sheet protein.²

In general, data analysis of vibrational studies is performed by fitting vibrational spectra. Once a vibrational spectrum is fit, the central frequencies of each vibrational band give information as to the frequencies that are enriched in the vibrational density of states, which then lead to conclusions about the local environments of the vibrational modes of interest. However, recent computational modeling of heterodyne phase-resolved chiral SFG spectra has produced predictions that do not seem to fit the assumptions of this workflow. In particular, our group demonstrated that the isolated O-H stretch response of the first hydration shell around the β-sheet protein LK₇β produces a characteristic "up-down" line shape [Fig. 1(a)],^{2,5,6} in contrast to the single peak of the infrared (IR)



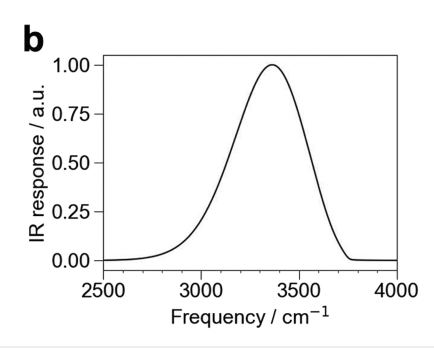


FIG. 1. Simulated vibrational spectra of water in the first hydration shell around LK₇β. (a) Chiral SFG (*psp*) response of water O–H stretch. (b) IR response of the same water molecules using the time-averaging approximation for a realistic peak width. ¹⁴ The spectrum in (a) was originally published in Ref. 2.

spectrum of the same ensemble of water [Fig. 1(b)]. It appears that the phase-resolved chiral SFG spectrum is not reporting directly the typical vibrational frequencies in the system. Thus, fitting the chiral SFG response of water with individual Lorentzian curves, as has been done so far, may not allow for the estimation of the underlying vibrational frequency distribution reliably and therefore may fall short in revealing structures and dynamics of water in the protein hydration shell. Hence, our computational results call into question whether the application of the standard assumptions in analyzing chiral SFG signals from water in hydration shells of biomolecules is valid.

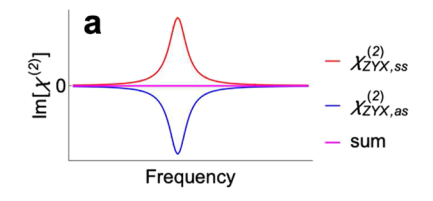
In this study, we demonstrate that the chiral SFG response of water around biomolecules is due to the incomplete cancellation of the responses of the symmetric and asymmetric stretching modes of water molecules. We show that the symmetric stretch response is the exact opposite of the asymmetric stretch response [Fig. 2(a)]. However, the symmetric and asymmetric stretch responses do not cancel because their frequencies are different due to intramolecular vibrational coupling and the variation in local environment of the two O-H groups within a single water molecule. Thus, their summation can lead to a nonzero "up-down" (or "down-up") chiral SFG signal [Fig. 2(b)]. It is worth noting that, while intermolecular couplings are present and significantly affect the spectral line shape for condensed-phase water, our previous work⁶ has shown that they do not significantly contribute to the chiral SFG spectral response. In that work, using an electric field mapping method, intramolecular coupling into symmetric and asymmetric vibrational modes was

found to be the dominant contribution to the chiral-specific SFG water line shape, with intermolecular coupling serving as an additional but relatively minor perturbation. This result was rationalized by considerations of symmetry, in which chiral SFG is symmetryallowed for the symmetric and asymmetric modes described by C_{2v} local symmetry of a water molecule, but not from spectrally isolated strongly H-bonded O-H local-mode contributions with nominal C_{∞} symmetry. This theoretical picture represented in Fig. 2(b) implies that the chiral SFG response of water provides an additional constraint to potentially improve curve fitting methods. Here, rather than fitting a separate Lorentzian curve to each O-H stretch feature, we fit water spectral responses with pairs of Lorentzian curves. Each pair of curves is with opposite phase, equal magnitude, and shifted frequencies. When applied to analyze our previously reported experimental chiral SFG spectra of β-sheet proteins,² method allows us to reduce the number of free parameters and extract more reliable frequency distributions from spectra, hence directly revealing the distribution of local environments experienced by the O-H groups of water in the biomolecular hydration shell.

THEORY

The chiral SFG signal arises from the molecular hyperpolarizability

Vibrational SFG spectra are produced by overlapping in space and time an infrared (IR) beam and a visible beam at an interfacial



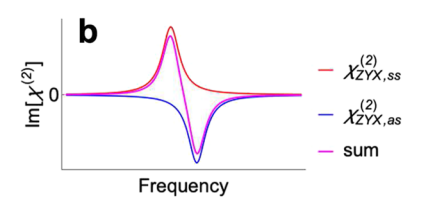


FIG. 2. The origin of the chiral SFG line shape for the water O–H stretch. (a) Zero chiral SFG response in the absence of both intramolecular coupling and differences in the local environment of the two O–H groups. (b) An "up-down" line shape in the presence of coupling and a frequency difference between the symmetric and asymmetric stretches. Subscripts ss and as stand for the symmetric stretch and asymmetric stretch responses, respectively. See Eq. (2) for the definition of $\chi^{(2)}_{ZYX}$, which is experimentally measured and computationally simulated to obtain chiral SFG spectra.

sample and measuring the sum frequency output. 15 Under the electric dipole approximation, the response of the system arises solely from the optical electric fields, which are given by

$$\vec{E}_{SFG} = E_{SFG}^X \hat{X} + E_{SFG}^Y \hat{Y} + E_{SFG}^Z \hat{Z}, \tag{1}$$

where $\hat{X},\,\hat{Y},$ and \hat{Z} are unit vectors corresponding to each coordinate axis in the laboratory frame and E_{SFG}^X , E_{SFG}^Y , and E_{SFG}^Z are the components of the electric field vector. Chiral SFG measures elements of the nonlinear response tensor $\chi^{(2)}$, a third-order tensor, which is defined by

$$E_{\rm SFG}^{I} = \sum_{IK} \chi_{IJK}^{(2)} E_{\rm vis}^{J} E_{\rm IR}^{K}, \tag{2}$$

where $E_{\rm vis}^J$ and $E_{\rm IR}^K$ are the components of the optical electric fields for the visible and IR beams, respectively, and I, J, and K range over the directions X, Y, and Z. The macroscopic $\chi^{(2)}$ emerges from an ensemble average of the microscopic molecular SFG response, the hyperpolarizability tensor β . For uniaxial interfacial assemblies, the orientation distribution in the azimuthal rotation angle ϕ can be assumed to be uniform, leading to

$$\chi_{IJK}^{(2)}(\theta, \psi) = \sum_{n} \frac{1}{2\pi} \int_{0}^{2\pi} d\phi_{n} \sum_{ijk} R_{Ii}^{n}(\phi_{n}, \theta_{n}, \psi_{n}) R_{Jj}^{n}(\phi_{n}, \theta_{n}, \psi_{n}) \times R_{Kk}^{n}(\phi_{n}, \theta_{n}, \psi_{n}) \beta_{ijk}^{n},$$
(3)

where β^n is the 27-element hyperpolarizability tensor of the *n*th molecule in the system; *i*, *j*, and *k* range over the three-dimensional Cartesian coordinates (x, y, z) of the molecular frame; \mathbb{R}^n is an Euler rotation matrix projecting the SFG response from the nth molecular frame to the laboratory frame; and ϕ_n , θ_n , and ψ_n are the Euler angles of the *n*th molecule projecting onto the laboratory coordinate (X, Y, and Z). The molecular hyperpolarizability (β) arises from the Raman tensor (α) and the transition dipole (μ) of the nth molecule according to 16

$$\beta_{ijk}^n \propto \alpha_{ij}^n \mu_k^n. \tag{4}$$

One of the surprising consequences of Eq. (3) is that some achiral chromophores exhibiting local mirror-plane symmetry in β may produce nonzero chiral $\chi^{(2)}$ elements, as outlined by the Simpson group. 12,13,18 This serves as a theoretical basis for chiral SFG methods probing hydration structures of biomolecules because it implies that achiral water molecules arranged in chiral superstructures at interfaces can produce chiral SFG signals. Thus, chiral SFG can selectively probe the biomolecular hydration shell without interference from bulk water. By manipulating the polarization of the IR and visible beams and the polarization setting for detecting SFG signals, particular components of $\chi^{(2)}$ can be isolated. For example, the *psp* polarization measures the response from the elements $\chi^{(2)}_{ZYX}$, $\chi_{XYZ}^{(2)}, \chi_{ZYZ}^{(2)}$, and $\chi_{XYX}^{(2)}, {}^{9,19}$ where p is the polarization on the incident plane and s is the polarization perpendicular to the incident plane, and the order of the notation of psp is for the SFG, visible, and IR beams, respectively. Of the four elements, only $\chi^{(2)}_{ZYX}$ survives in a uniaxial system with C_{∞} symmetry and in the absence of electronic resonance. Hence, we measure $\chi^{(2)}_{ZYX}$ in our chiral SFG experiments

under the conditions of electronic nonresonance and compute $\chi_{ZYX}^{(2)}$ to simulate chiral SFG spectra.

The chiral SFG symmetric and asymmetric stretch responses are opposite in sign

In order to validate the model that explains the "up-down" (or "down-up") line shape of the chiral SFG response of water as represented in Fig. 2(b), we must prove that (1) the symmetric and asymmetric stretches are at different frequencies and (2) the symmetric and asymmetric stretches of water chiral SFG responses are equal but have opposite signs. Point 1 is known to be true, as intramolecular coupling and differences in the local environments of the two O-H groups in a water molecule cause the symmetric and asymmetric stretches to be non-degenerate. Therefore, we need to prove point 2,

$$\chi_{ZYX ss}^{(2)} = -\chi_{ZYX ss}^{(2)} \tag{5}$$

where "ss" refers to the symmetric stretch and "as" to the asymmetric stretch. To do so, we define four frames of reference (Fig. 3). They include two frames corresponding to two O–H groups: (a_1, b_1, c_1) and (a_2, b_2, c_2) , one frame corresponding to the entire water molecule: (x, y, z), and the laboratory frame: (X, Y, Z). In the two O-H frames [Fig. 3(a)], the corresponding c_1 axis and c_2 axis point along the O-H bonds. In the molecular frame [Fig. 3(b)], the z axis points along the bisector of the H–O–H angle and the x axis is in the H–O–H plane. In the laboratory frame, the Z axis is perpendicular to the interface defining the uniaxial system and the *X* and *Y* axes point along the surface.

For water in the C_{2v} point group, the symmetric stretch corresponds to the A₁ irreducible representation and the asymmetric stretch corresponds to the B₁ irreducible representation for the coordinate system shown in Fig. 3(b). The corresponding elements of the molecular hyperpolarizability are $\beta_{\rm H_2O}^{zzz}$, $\beta_{\rm H_2O}^{xxz}$, and $\beta_{\rm H_2O}^{\tilde{y}yz}$ for the symmetric stretch and $\beta_{H_2O}^{xzx}$ and $\beta_{H_2O}^{zxx}$ for the asymmetric stretch. In a uniaxial system of C_{2v} molecules, following Eq. (3), the chiral SFG response is given by69

$$\chi_{ZYX}^{(2)} = \frac{1}{2}\sin^2\theta \sin\psi \cos\psi(-\beta_{H_2O}^{xxz} + \beta_{H_2O}^{yyz} + \beta_{H_2O}^{xzx}).$$
 (6)

Therefore, the symmetric stretch contribution is

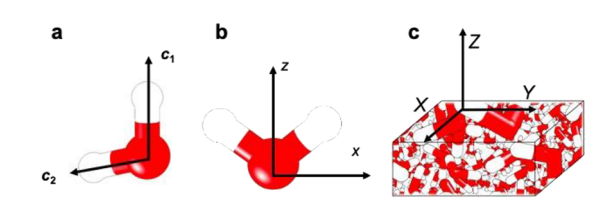


FIG. 3. The four coordinate systems used in the derivation: (a) the two O-H frames $(a_1, b_1, \text{ and } c_1)$ and $(a_2, b_2, \text{ and } c_2)$, (b) the molecular frame (x, y, z), and (c) the laboratory frame (X, Y, Z).

$$\chi_{ZYX,ss}^{(2)} = \frac{1}{2} \sin^2 \theta \sin \psi \cos \psi \left(-\beta_{H_2O}^{xxz} + \beta_{H_2O}^{yyz} \right), \tag{7}$$

and the asymmetric stretch contribution is

$$\chi_{ZYX,as}^{(2)} = \frac{1}{2}\sin^2\theta \sin\psi \cos\psi(\beta_{H_2O}^{xzx}). \tag{8}$$

Relationships between these symmetric and asymmetric tensor contributions can be further simplified by considering the intramolecular coupling as a relatively minor perturbation to a system of two uncoupled local-mode O-H stretching motions. We can then express the molecular hyperpolarizability β elements in Eq. (6) in terms of the surviving hyperpolarizability elements in the two O-H frames illustrated in Fig. 3(a). Prior to "turning on" coupling, each of the individual O–H motions is linear (local C_{∞} -symmetry). Hence, the only surviving elements are β_{OHi}^{ccc} and $\beta_{OHi}^{aac} = \beta_{OHi}^{bbc}$, where i = 1 or 2 [Fig. 3(a)]. In this perturbation theoretical framework, the signs and magnitudes of the symmetric and asymmetric motions can be generated by projecting the local-mode O-H motions from the two separate O-H bond frames (a_1, b_1, c_1) and (a_2, b_2, c_2) [Fig. 3(a)] to the water molecular frame (x, y, z) [Fig. 3(b)]. The first O-H frame is related to the molecular frame by the transformation matrix of

$$S_{1} = \begin{pmatrix} \cos \theta' & 0 & \sin \theta' \\ 0 & 1 & 0 \\ -\sin \theta' & 0 & \cos \theta' \end{pmatrix}, \tag{9}$$

where $\theta' = 52.25^{\circ}$, which is the angle between the c_1 axis and z axis (Fig. 3) and half the water molecule's H–O–H angle. The second O–H frame is related to the molecular frame with an opposite direction of rotation by the transformation matrix of

$$S_2 = \begin{pmatrix} \cos \theta' & 0 & -\sin \theta' \\ 0 & 1 & 0 \\ \sin \theta' & 0 & \cos \theta' \end{pmatrix}. \tag{10}$$

Hence, the molecular hyperpolarizability $\beta_{\rm H_2O}$ can be expressed in terms of $\beta_{\rm OH1}$ and $\beta_{\rm OH2}$,

$$\beta_{\text{H}_{2}\text{O}}^{ijk} = S_{1}^{ii'} S_{1}^{jj'} S_{1}^{kk'} \beta_{\text{OH}_{1}}^{i'j'k'} + S_{2}^{ii'} S_{2}^{jj'} S_{2}^{kk'} \beta_{\text{OH}_{2}}^{i'j'k'}, \tag{11}$$

where i, j, and k range over the molecular coordinates x, y, and z and i', j', and k' range over the OH bond coordinates a, b, and c. Thus, we can obtain

$$\begin{split} \beta_{\text{H}_{2}\text{O}}^{yyz} &= \left(S_{1}^{yc} S_{1}^{yc} S_{1}^{cc} \beta_{\text{OH}_{1}}^{ccc} + S_{2}^{yc} S_{2}^{yc} \beta_{\text{OH}_{2}}^{ccc} \right) + \left(S_{1}^{ya} S_{1}^{ya} S_{1}^{aac} \beta_{\text{OH}_{1}}^{aac} + S_{2}^{ya} S_{2}^{ya} S_{2}^{cc} \beta_{\text{OH}_{2}}^{aac} \right) + \left(S_{1}^{yb} S_{1}^{yb} S_{1}^{zc} \beta_{\text{OH}_{1}}^{bbc} + S_{2}^{yb} S_{2}^{yc} \beta_{\text{OH}_{2}}^{bbc} \right) \\ &= 0 + 0 + 0 + 0 + \cos \theta' \beta_{\text{OH}_{1}}^{aac} + \cos \theta' \beta_{\text{OH}_{2}}^{aac} \\ &= \cos \theta' \left(\beta_{\text{OH}_{1}}^{aac} + \beta_{\text{OH}_{2}}^{aac} \right), \end{split}$$
(12)

$$\begin{split} \beta_{\rm H_2O}^{xxz} &= \left(S_1^{xc} S_1^{xc} S_1^{zc} \beta_{\rm OH1}^{ccc} + S_2^{xc} S_2^{zc} \beta_{\rm OH2}^{ccc} \right) + \left(S_1^{xa} S_1^{xa} S_1^{zc} \beta_{\rm OH1}^{aac} + S_2^{xa} S_2^{zc} \beta_{\rm OH2}^{aac} \right) + \left(S_1^{xb} S_1^{xb} S_1^{zc} \beta_{\rm OH1}^{bbc} + S_2^{xb} S_2^{xb} S_2^{zc} \beta_{\rm OH2}^{bbc} \right) \\ &= \sin^2 \theta' \, \cos \theta' \beta_{\rm OH1}^{ccc} + \sin^2 \theta' \, \cos \theta' \beta_{\rm OH2}^{ccc} + \cos^3 \theta' \beta_{\rm OH1}^{aac} + \cos^3 \theta' \beta_{\rm OH2}^{aac} + 0 + 0 \\ &= \sin^2 \theta' \, \cos \theta' \left(\beta_{\rm OH1}^{ccc} + \beta_{\rm OH2}^{ccc} \right) + \cos^3 \theta' \left(\beta_{\rm OH1}^{aac} + \beta_{\rm OH2}^{aac} \right) \\ &= \sin^2 \theta' \, \cos \theta' \left(\beta_{\rm OH1}^{ccc} + \beta_{\rm OH2}^{ccc} \right) + \cos \theta' \left(1 - \cos^2 \theta' \right) \left(\beta_{\rm OH1}^{aac} + \beta_{\rm OH2}^{aac} \right) \\ &= \sin^2 \theta' \, \cos \theta' \left(\beta_{\rm OH1}^{ccc} + \beta_{\rm OH2}^{ccc} \right) - \left(\beta_{\rm OH1}^{aac} + \beta_{\rm OH2}^{aac} \right) \right] + \cos \theta' \left(\beta_{\rm OH1}^{aac} + \beta_{\rm OH2}^{aac} \right), \end{split}$$

$$(13)$$

$$\beta_{\text{H}_{2}\text{O}}^{xzx} = \left(S_{1}^{xc} S_{1}^{zc} S_{1}^{xc} \beta_{\text{OH}_{1}}^{ccc} + S_{2}^{xc} S_{2}^{zc} \beta_{\text{OH}_{2}}^{ccc}\right) + \left(S_{1}^{xa} S_{1}^{za} S_{1}^{xc} \beta_{\text{OH}_{1}}^{aac} + S_{2}^{xa} S_{2}^{za} S_{2}^{xc} \beta_{\text{OH}_{2}}^{aac}\right) + \left(S_{1}^{xb} S_{1}^{zb} S_{1}^{xc} \beta_{\text{OH}_{1}}^{bbc} + S_{2}^{xb} S_{2}^{zb} S_{2}^{xc} \beta_{\text{OH}_{2}}^{bbc}\right)$$

$$= \sin^{2} \theta' \cos \theta' \beta_{\text{OH}_{1}}^{ccc} + \sin^{2} \theta' \cos \theta' \beta_{\text{OH}_{2}}^{ccc} + \cos \theta' \left(-\sin \theta'\right) \sin \theta' \beta_{\text{OH}_{1}}^{aac} + \cos \theta' \left(-\sin \theta'\right) \beta_{\text{OH}_{2}}^{aac} + 0 + 0$$

$$= \sin^{2} \theta' \cos \theta' \left[\left(\beta_{\text{OH}_{1}}^{ccc} + \beta_{\text{OH}_{2}}^{ccc}\right) - \left(\beta_{\text{OH}_{1}}^{aac} + \beta_{\text{OH}_{2}}^{aac}\right)\right]. \tag{14}$$

Substituting Eqs. (12)–(14) into Eqs. (7) and (8) shows that the symmetric and asymmetric stretch signals from a water molecule are equal but opposite [Eq. (5)]. This statement is true whether or not the two O–H groups have equivalent hyperpolarizabilities, and thus, it is applicable to water molecules in complex, heterogeneous environments.

This result seems to imply that the total chiral signal is zero. However, in reality, the symmetric and asymmetric signals are shifted in frequency relative to one another due to both vibrational coupling and heterogeneous local environments. The asymmetric component is typically assumed to have the higher frequency because the average intramolecular coupling is negative. Hence, the symmetric and asymmetric responses do not perfectly cancel, and instead, they produce a characteristic two-peak line shape [Fig. 2(b)]. This two-peak line shape can be "up-down" or "down-up." When the symmetric stretch response is positive and the asymmetric stretch is negative, the line shape will be "up-down" [Fig. 2(b)] and vice versa for a "down-up" line shape.

Fitting experimental chiral SFG spectra with pairs of Lorentzian curves

The breakdown of the chiral SFG signal of individual water molecules into symmetric and asymmetric components implies that one needs to derive a new functional form to fit the heterodyne chiral SFG spectra of water. This will allow for extracting information about the underlying frequency distribution that can reveal molecular interactions of water. The functional form for a pair of water O–H stretching peaks should contain a pair of opposite Lorentzian curves with equal amplitude and a frequency displacement, as in

$$f(\omega) = \operatorname{Im}\left[\frac{A}{\omega - \left(\nu - \frac{1}{2}\Delta\nu\right) - i\Gamma} + \frac{-A}{\omega - \left(\nu + \frac{1}{2}\Delta\nu\right) - i\Gamma}\right], \quad (15)$$

where ω is the IR frequency, A is the amplitude of the pair, v is the frequency of the midpoint between the two Lorentzian curves, Δv is the difference in frequency between the two Lorentzian curves, and Γ relates to the peak width. This functional form involves fewer free parameters in fitting the chiral SFG spectra of water, as fitting two Lorentzian curves requires six parameters (two amplitudes, two widths, and two centers), whereas the new functional form requires only four (one amplitude, one width, center frequency, and a frequency difference). Fitting to a pair of opposite curves yields one center frequency instead of two, thus producing a single peak in the

frequency distribution, which is consistent with the IR spectrum of first hydration shell water [Fig. 1(b)].

The experimental spectra contain contributions of N–H stretches from the protein and O–H stretches from water. The water contributions can be described by the functional form in Eq. (15), while the protein contributions can be still described by individual Lorentzian functions. Hence, a linear combination of Eq. (15) for the water contributions and individual Lorentzian functions for the protein contributions can be used to fit the experimental spectra,

$$f(\omega) = \operatorname{Im}\left[\sum_{m} \frac{A_{m}}{\omega - \nu_{m} - i\Gamma_{m}}\right] + \operatorname{Im}\left[\sum_{n} \frac{A_{n}}{\omega - \left(\nu_{n} - \frac{1}{2}\Delta\nu_{n}\right) - i\Gamma_{n}}\right] + \frac{-A_{n}}{\omega - \left(\nu_{n} + \frac{1}{2}\Delta\nu_{n}\right) - i\Gamma_{n}}\right],$$
(16)

where v_n is the resonant frequency of the nth pair of water peaks, v_m is the resonant frequency of the mth unpaired protein peak, A_n and A_m are the corresponding amplitudes, Γ_n and Γ_m are the corresponding damping coefficients, and Δv_n is the difference in frequency for the nth water symmetric and asymmetric stretches.

To fit the experimental spectra, we cannot treat the frequency difference between the symmetric and asymmetric stretches of water (Δv) as a pure fitting variable. Doing so often yields meaningless results because the value can become so large that the peaks in

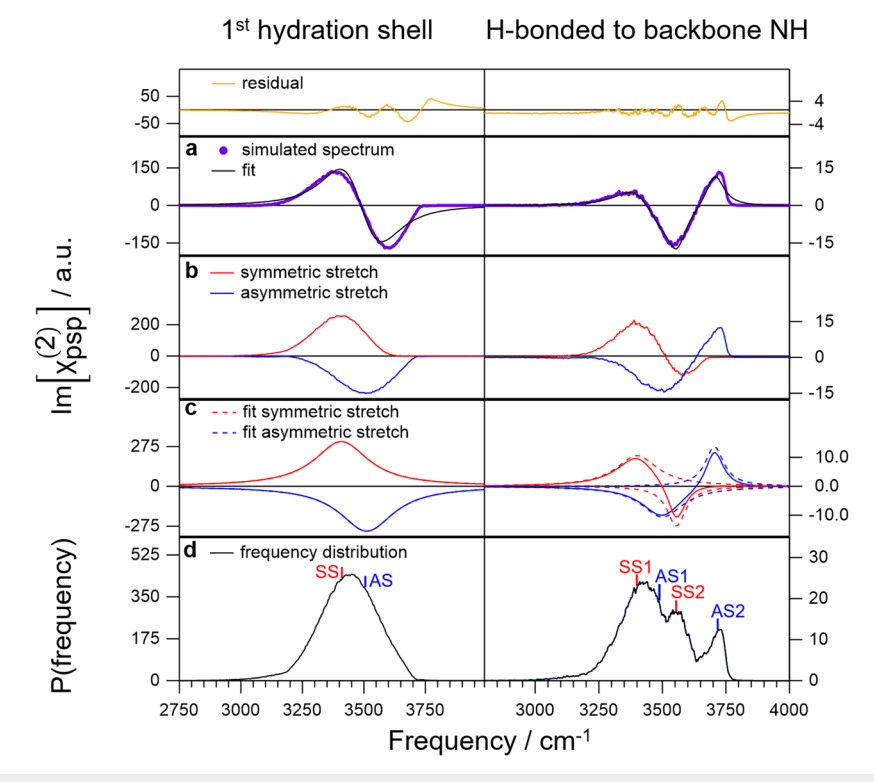


FIG. 4. Lorentzian pair-based fits to the computed O–H stretch chiral SFG response for the first hydration shell around $LK_7β$ (left) and the subset of water molecules hydrogen-bonded to N–H groups on the protein backbone (right). (a) Total fits to the simulated spectra with the residual plotted at the top in yellow. (b) Simulated symmetric and asymmetric stretch responses. (c) Symmetric and asymmetric stretch responses (solid lines) obtained from the fit, where the dashed lines on the right indicate component peaks of two Lorentzian pairs. (d) Frequency distributions obtained from the fit. The spectra in (a) were originally published in the work of Konstantinovsky *et al.*²

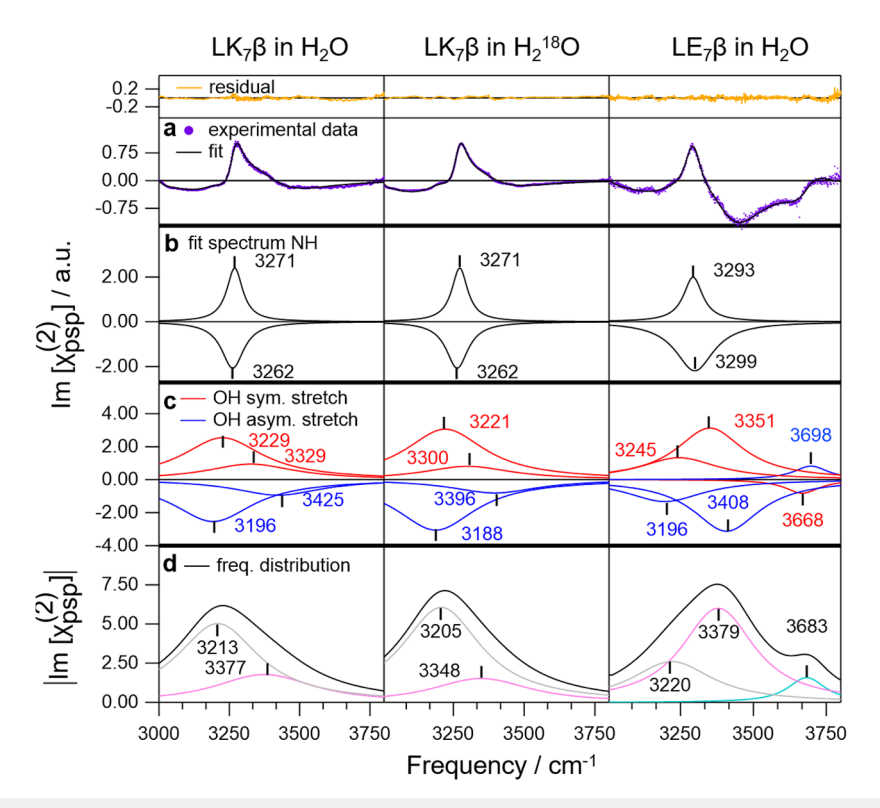


FIG. 5. Fitting of experimental spectra. (a) Experimental heterodyne chiral SFG spectra (purple dots) and fits (solid lines) for LK₇β in H₂O (left column) and H₂¹⁸O (center column) and LE₇β in H₂O (right column) with the residuals displayed at the top in yellow. (b) The Lorentzian peaks used to fit the N–H stretching modes. (c) The paired Lorentzian peaks used to fit the O–H symmetric (red) and asymmetric (blue) stretches. (d) The O–H stretch frequency distribution (black lines) with the component frequency distributions in pink, gray, and cyan, where each labeled frequency corresponds to the center of a pair of symmetric and asymmetric stretches in (c). The spectra in (a) were previously published in the work of Konstantinovsky *et al.*^{2,21}

the pair are completely independent or so small that the fit curve becomes a baseline due to cancellation of the two peaks that are equal in amplitude but opposite in sign. To address this issue, we need to constrain the value of Δv . This value depends on the fundamental water O–H stretching frequencies and the intramolecular coupling strength, which can be calculated by the ensemble average for a subset of vibrational chromophores. Based on the analysis of the simulated symmetric and asymmetric stretches of the subsets shown in Figs. 4 and S1–S7, we constrain the value of Δv to be in the range of 30–150 cm⁻¹. With this constraint, we fit the experimental spectra and present the fitting results in Fig. 5 and Tables S1 and S2.

RESULTS AND DISCUSSION

We validate our new fitting method [Eq. (16)] by analyzing previously reported computational and experimental spectra of hydration water around the model protein systems LK₇ β and LE₇ β , ^{2,5,21} which have sequences Ac-LKLKLKL-NH₂ and Ac-LELELEL-NH₂, respectively. They fold into amphiphilic, antiparallel β -sheets at the air–water interface, making them ideal for chiral SFG studies. ^{22–26} The hydrophobic leucine residues (L) point into the air, while the positively charged lysine (K) or the negatively charged glutamate

(E) residues point into the water. It should be noted that the results presented here apply to other systems, including other proteins and even non-protein systems (e.g., DNA¹), because the main result concerns the chiral water response rather than the response of a specific biomolecule. Therefore, the proof of the model that explains the updown (or down-up) line shape [Eq. (5) and Fig. 2(b)] remains valid regardless of the chemical identity of the biomolecules.

Lorentzian-pair-based fitting agrees with calculated chiral SFG spectra

We start validating our model by decomposing the simulated chiral SFG spectra of water into symmetric and asymmetric O–H stretch components and then comparing them to the results of fitting the computational spectra with the new functional form [Eq. (16)]. We calculate the O–H stretch spectra of all water molecules in the first hydration shell of LK7 β and a subset of these water molecules that are hydrogen-bonded to the peptide backbone of LK7 β (Fig. 4). The separation of symmetric and asymmetric stretch contributions is accomplished by adapting the Skinner group's inhomogeneous limit approximation approach $^{14,27-30}$ to calculate chiral SFG spectra. In this case, the SFG response is approximately given by

$$\chi_{IJK}^{(2)}(\omega) \approx \left| \sum_{a=1}^{N_{\text{OH}}} \frac{\sum_{b=1}^{N_{\text{OH}}} U_{ba} \alpha_b^{IJ} \sum_{b=1}^{N_{\text{OH}}} U_{ba} \mu_b^K}{\lambda_a - \omega - \frac{i}{2\tau}} \right|, \tag{17}$$

where α_b^{IJ} is the IJth element of the Raman polarizability tensor of the bth O–H group, μ_b^K is the Kth element of the transition dipole of the bth O–H group, \mathbf{U} is the eigenvector matrix of the exciton Hamiltonian, and λ is the eigenvalue vector of the exciton Hamiltonian. Here, τ is the vibrational decay lifetime, fixed at 1.3 ps in our calculations.³¹ The average is over all configurations in a molecular dynamics (MD) simulation. The elements of the exciton Hamiltonian, ^{20,31–36} which has vibrational frequencies on the diagonal and vibrational couplings on the off-diagonal, and the transition polarizability and dipole are computed using the Skinner group's electrostatic map relating local electric fields to these quantities, as we have used in past studies. ^{14,20,31,33,34,37}

We devise a method to isolate the symmetric or asymmetric stretch components. If intermolecular couplings are neglected, the eigenvectors of the exciton Hamiltonian have the form

$$\vec{\mathbf{e}}_a = (0 \quad 0 \quad \cdots \quad x \quad y \quad \cdots \quad 0 \quad 0), \tag{18}$$

where x and y can be both positive, both negative, or of opposite signs. If x and y have the same sign, we consider the eigenvector to belong to the symmetric stretch, and the symmetric stretch response is given by

$$\chi_{IJK}^{(2)}(\omega) \approx \left(\sum_{a \in \text{symm}}^{N_{\text{OH}}} \frac{\sum_{b=1}^{N_{\text{OH}}} U_{ba} \alpha_b^{JJ} \sum_{b=1}^{N_{\text{OH}}} U_{ba} \mu_b^K}{\lambda_a - \omega - \frac{i}{2\tau}} \right). \tag{19}$$

We calculate the asymmetric stretch response similarly by considering only those eigenvectors where x and y are of opposite sign. Notably, the asymmetric and symmetric stretch responses in the calculations are not exactly opposite because of the difference in symmetric and asymmetric frequency eigenvalues that arises from coupling.

In a recent publication, we calculated the chiral SFG response of various subsets of water molecules in the first hydration shell around $LK_7\beta$.² We now apply our new fitting strategy to the computed chiral response of two subsets: the entire first hydration shell and the water molecules hydrogen-bonded to the N-H groups on the protein backbone within the first hydration shell (similar analyses of the other subsets are presented in the supplementary material). The chiral SFG response of these two subsets is shown in Fig. 4(a) (purple). We chose these two subsets because they represent well the range of line shapes encountered when calculating the chiral response of various groups of water molecules around LK₇ β .² The first hydration shell response is relatively simple [Fig. 4(a), left], whereas the N-H-bound water molecules produce a more complicated line shape [Fig. 4(a), right]. We first calculated the symmetric and asymmetric stretch chiral SFG responses [Fig. 4(b)], as detailed above. We then fit the signals [black solid lines, Fig. 4(a)] with the residuals of the fitting shown above Fig. 4(a) (yellow solid lines). The signal of the first hydration shell subset is fit with a single pair of peaks [left, dashed lines, Fig. 4(c)], and the signal of the water subset hydrogen-bonded to N-H groups is fit with two pairs [right, dashed

lines, Fig. 4(c)]. We chose to fit the spectra with a minimal number of pairs to avoid overfitting.

Each pair of peaks is given by two Lorentzians of opposite sign, as in Eq. (15). In the fit to the first hydration shell spectrum [left column, Fig. 4(a)], Δv was taken to be 100 cm⁻¹ based on the simulated symmetric and asymmetric stretch results [left column, Fig. 4(b)], and A, ν , and Γ were free parameters. In the fit to the N-H-bound water spectrum [right column, Fig. 4(a)], we used 100 cm⁻¹ for the lower frequency pair and obtained 150 cm⁻¹ for the higher frequency pair from the fitting [right column, Fig. 4(a)]. We identify the symmetric and asymmetric stretch components from the fit [red and blue lines, Fig. 4(c)] using the knowledge that the asymmetric stretch has a higher frequency than the symmetric stretch because the typical intramolecular coupling is negative. 6,20 Accordingly, we can add all symmetric contributions [red dashed lines, Fig. 4(c)] from the fit to yield the total symmetric response [red solid line, Fig. 4(c)]. Similarly, we can also add all asymmetric contributions [blue dashed lines, Fig. 4(c)] to obtain the total asymmetric response [blue solid line, Fig. 4(c)]. The solid and dashed lines overlap in Fig. 4(c) (left) because there is only one pair of water peaks. These total asymmetric and symmetric responses obtained from the fitting [solid lines, Fig. 4(c)] appear to agree well with the total asymmetric and symmetric responses [Fig. 4(b)] derived purely from the simulations based on the theory described in Eq. (19). This agreement provides evidence to support the model [Fig. 2(b)] that explains the two-peak "up-down" (or "down-up") line shape of the chiral SFG response of water molecules.

We estimate the frequency distribution of chiral water superstructures [Fig. 4(d)] by adding the absolute values of the computationally predicted symmetric and asymmetric stretch components. We find that the first hydration shell subset has a single-peak frequency distribution. This is consistent with the IR spectrum in Fig. 1(b), which has a single peak around 3400 cm⁻¹, and is very similar to that of bulk water.³⁷ This is consistent with our previous argument that water molecules around a protein experience a similar environment to bulk water in terms of hydrogen bonding environment.² Whatever environment a water molecule experiences, it tries to form three to four hydrogen bonds. Furthermore, our calculations and fitting reveal that in the subset of water hydrogen-bonded to the peptide backbone N-H, the peak at the highest frequency is solely due to the asymmetric stretch component [Figs. 4(b)-4(d), right]. We previously proposed that this high-frequency peak is due to water molecules containing one O-H group pointing into the air and another hydrogen bonded to an N-H group on the backbone.² We now understand that this peak is due to the asymmetric-stretch half of a pair centered at ~3650 cm⁻¹ [Fig. 4(c), right]. This interpretation indicates that the water molecules producing this pair of water peaks are not hydrogen-bond free but most likely experience some degree of hydrogen bonding with both of their O-H groups, although this hydrogen bonding is weak. Hence, the water molecules in this subset do not have O-H groups pointing directly toward the air, as that would most likely push the peak pair's central frequency above 3700 cm⁻¹. The corresponding symmetric stretch peak in the high-frequency pair [Fig. 4(c), right] is negative and buried in the total line shape. This analysis illustrates a subtlety of heterodyne chiral SFG—peaks can cancel and obscure each other due to the nature of the positive- and negative-phase response. In addition, a peak in the frequency distribution [Fig. 4(d)] does not necessarily indicate a

peak *pair* center near the peak's frequency. The asymmetric stretch response may be pushed to a high frequency by intramolecular coupling effects rather than O–H groups facing into the air. Moreover, the peak in Fig. 4(d) (right) at around 3450 cm⁻¹ is primarily due to the positive symmetric stretch (red) in Fig. 4(b) (right). The middle peak in Fig. 4(d) (right) at around 3550 cm⁻¹ is due to the negative peaks of both symmetric (red) and asymmetric (blue) stretches in Fig. 4(b) (right).

We fit the spectra of seven other water subsets reported in the work of Konstantinovsky *et al.*² (Figs. S1–S7). These subsets include (1) water associated with the backbone of LK₇ β , (2) water associated with sidechains, (3) water molecules in the backbone subset but not forming hydrogen bonds with the protein, (4) water hydrogen-bonded to carbonyl groups on the backbone, (5) water forming very short hydrogen bonds with the carbonyl groups on the backbone (a distance of <1.6 Å between hydrogen and acceptor), (6) water molecules in the sidechain subset but not making hydrogen bonds to the protein, and (7) water molecules hydrogen-bonded to lysine sidechains. We have obtained very similar results. Altogether, these analyses validate our model [Fig. 2(b)] and illustrate the advantage of the new fitting approach. Based on these analyses, we can now infer frequency distributions from chiral SFG spectra and interpret the physical meaning of peak locations.

The new model allows fitting of experimental spectra for estimating the vibrational frequency distribution

We next apply the new fitting strategy [Eq. (16)] to analyze our previously published experimental heterodyne chiral SFG The O-H-stretch peaks were identified using isotopic labeling with H₂¹⁸O, which is expected to make O-H-dominated peaks red-shift by ~12 cm⁻¹.^{2,5} Peaks due to the N-H stretch were fit with conventional Lorentzians (one peak per feature). Figure 5 shows fits for experimental chiral SFG spectra of $LK_7\beta$ in H_2O (left column), LK₇β in H₂¹⁸O (central column), and LE₇β in H₂O (right column). The experimental spectra and their overall fits are shown in Fig. 5(a), the fitted Lorentzians for N-H stretches in Fig. 5(b), the fitted pairs of Lorentzians for O-H stretches in Fig. 5(c), and the estimated frequency distribution in Fig. 5(d). The residuals from the overall fits are plotted in yellow above Fig. 5(a). As seen from Fig. 5(a) and the residuals, the fits are quite satisfactory, and the ${\rm H_2}^{18}{\rm O}$ -induced red shifts are also captured. To obtain a similarly good fit for LK₇β using the standard approach, a total of seven Lorentzian peaks and 21 free parameters were needed (Fig. S8, Tables S1-S4), whereas here only 14 free parameters were used. Thus, our new fitting strategy can reduce the ambiguity of spectral analysis, improving the molecular understanding of the biomolecules and their hydration structures.

We obtain the approximate frequency distribution by adding the absolute values of the symmetric and asymmetric stretch contributions [Fig. 5(d)]. The distribution appears to be more reliable than that estimated from the conventional fit [Fig. S8(a)]. The highly jagged nature of the frequency distribution obtained using the previous conventional fit [Fig. S8(d)] does not match the smooth nature of the calculated IR response [Fig. 1(b)], while the frequency distribution obtained using the new fitting strategy is smoother. Isotopic labeling with $H_2^{18}O$ causes red shifts in the frequency distribution of the water around $LK_7\beta$, as expected. By contrast, the conventional

fits show drastically different frequency distributions for $\rm H_2O$ and $\rm H_2^{18}O$ (Fig. S8), failing to reveal the expected isotopic shifts. This observation again validates the new fitting strategy for providing a molecular interpretation of chiral SFG spectra of water.

The frequency distribution of OH stretches around LK₇β is composed of two component peaks [the first and second columns, Fig. 5(d)], whereas the distribution around LE₇ β is composed of three component peaks [the third column, Fig. 5(d)], including an emergent peak at a very high frequency (3683 cm⁻¹). This peak is most likely due to water molecules interacting weakly with the protein, perhaps with one OH group facing the air. We presume that such molecules also exist in the $LK_7\beta$ system. However, because the protein-hydration shell interactions are stronger in the LK₇ β system relative to the LE₇ β system, as shown previously,²¹ these water molecules may contribute relatively less to the total aqueous response. It is important to note that a water molecule need not be strongly hydrogen-bonded to the protein to be part of a stable chiral hydration structure. The low frequencies in the frequency distribution around $LK_7\beta$ may correspond partially to water molecules that are geometrically constrained by the stable protein structure and as a result form strong hydrogen bonds with other water molecules in the first hydration shell. Hence, chiral SFG is not only a reporter of hydrogen bond strength in the first hydration shell but also of the geometric, collective order of water molecules around the chiral biomolecular scaffolds.

The frequency distributions in Fig. 5(d) show that LE₇ β has a significantly blue-shifted distribution of water compared to LK₇β, suggesting weaker hydrogen bonds of water surrounding the protein. This is consistent with past findings of molecular dynamics studies that $LE_7\beta$ is less stable than $LK_7\beta$ in terms of backbone hydrogen bonds.²¹ Our prior experiments show that the main N-H peak is blue-shifted in LE₇β (Fig. S8). This dominant N-H contribution masks the O-H peaks, and thus, the O-H stretch frequencies remained elusive in the analysis using the conventional fitting method (Fig. S8). The new fitting clearly shows that the water signal is also blue-shifted in the experimental spectra, unveiling agreement with previously reported computational O-H stretch spectra.³⁸ These blue shifts of water O-H stretches and protein N-H stretches reveal that $LE_7\beta$ has a relatively lower ability to form a coherent water supramolecular structure and is less stable intrinsically. Although our previous molecular dynamics studies already demonstrated the correlation between water O-H stretches and protein N-H stretches,21 the new fitting model allows us to reliably extract the O-H stretching frequencies of water in the first hydration shell from experiments, thereby validating the correlation. This combined experimental and computational result has a profound implication—the stability of a protein and its hydration shell can be intimately connected.

CONCLUSION

We have used a theoretical insight regarding the relationship between the symmetric and asymmetric stretch chiral SFG responses of water to devise a new strategy for fitting chiral SFG spectra and extracting frequency distributions. We have shown that the characteristic "up-down" or "down-up" line shape of the O–H stretch response of chiral water superstructures is due to the incomplete cancellation of opposite-phase symmetric and asymmetric stretch

components. We previously showed that O-H/N-H coupling is critical to the modeling of the N-H stretch component of the SFG spectra of $LK_7\beta$ and $LE_7\beta$.²¹ Thus, future investigations will need to incorporate the effects of intermolecular coupling. Although we consider only intramolecular coupling as a first approximation in this study, we have shown that the theory derived within this approximation introduces a new strategy for analyzing the experimental and computational spectra. This strategy allows for spectral interpretation to extract molecular information. The application of our theoretical model for analyzing previous experimental data has captured the isotopic shifts of water O-H stretches and revealed physical pictures of a correlation between protein stability and hydrogen-bonding interactions of water in the first hydration shell. It is possible that similar insights can be developed for other types of vibrational spectroscopy or other molecular systems, enabling more insightful analysis of experimental spectra and a better understanding of computational results.

SUPPLEMENTARY MATERIAL

See the supplementary material for original fits to experimental data, fits to the computational spectra for seven other water subsets around LK₇β, and table of fitting parameters for all experimental data fits.

ACKNOWLEDGMENTS

The authors wish to thank Dr. Pablo Videla of Yale University for the VMD scripts to set up $LK_7\beta$ and $LE_7\beta$. This work was supported by the National Institutes of Health under Grant No. R35 GM139449 (S.H.-S.) and the National Science Foundation under Grant No. CHE-2108690 (E.C.Y.Y.). D.K. was supported by these grants. M.T. was supported by NIH Grant No. R35 GM139449 (S.H.-S.). T.S. was supported by Grant No. CHE-2108690 (to E.C.Y.Y.). G.J.S. gratefully acknowledges financial support for this work from the National Science Foundation (Grant Nos. NSF-CMI 2305178, NSF-MRI-ID 2320751, and NSF-CMI 2004046).

AUTHOR DECLARATIONS

Conflict of Interest

The authors have no conflicts to disclose.

Author Contributions

D.K. and T.S. contributed equally to this work.

Daniel Konstantinovsky: Conceptualization (equal); Data curation (equal); Formal analysis (equal); Investigation (equal); Methodology (equal); Validation (equal); Visualization (equal); Writing - original draft (equal); Writing - review & editing (equal). Ty Santiago: Data curation (equal); Formal analysis (equal); Investigation (equal); Methodology (equal); Validation (equal); Visualization (equal); Writing - original draft (equal); Writing - review & editing (equal). Matthew Tremblay: Data curation (equal); Formal analysis (equal); Investigation (equal); Methodology (equal); Validation

(equal); Visualization (equal); Writing – original draft (equal); Writing - review & editing (equal). Garth J. Simpson: Conceptualization (equal); Funding acquisition (equal); Investigation (equal); Methodology (equal); Validation (equal); Writing – review & editing (equal). Sharon Hammes-Schiffer: Conceptualization (equal); Funding acquisition (equal); Investigation (equal); Methodology (equal); Project administration (equal); Supervision (equal); Validation (equal); Writing - review & editing (equal). Elsa C. Y. Yan: Conceptualization (equal); Funding acquisition (equal); Investigation (equal); Project administration (equal); Supervision (equal); Validation (equal); Writing - original draft (equal); Writing - review & editing (equal).

DATA AVAILABILITY

The data that support the findings of this study are available within the article and its supplementary material.

REFERENCES

- ¹M. L. McDermott, H. Vanselous, S. A. Corcelli, and P. B. Petersen, "DNA's chiral spine of hydration," ACS Cent. Sci. 3(7), 708-714 (2017).
- ²D. Konstantinovsky, E. A. Perets, T. Santiago, L. Velarde, S. Hammes-Schiffer, and E. C. Y. Yan, "Detecting the first hydration shell structure around biomolecules at interfaces," ACS Cent. Sci. 8(10), 1404-1414 (2022).
- ³E. A. Perets and E. C. Y. Yan, "Chiral water superstructures around antiparallel β-sheets observed by chiral vibrational sum frequency generation spectroscopy," J. Phys. Chem. Lett. 10(12), 3395–3401 (2019).
- ⁴E. C. Y. Yan, E. A. Perets, D. Konstantinovsky, and S. Hammes-Schiffer, "Detecting interplay of chirality, water, and interfaces for elucidating biological functions," Acc. Chem. Res. 56(12), 1494-1504 (2023).
- ⁵E. A. Perets, D. Konstantinovsky, L. Fu, J. Chen, H.-F. Wang, S. Hammes-Schiffer, and E. C. Y. Yan, "Mirror-image antiparallel β-sheets organize water molecules into superstructures of opposite chirality," Proc. Natl. Acad. Sci. U. S. A. 117(52), 32902-32909 (2020).
- ⁶D. Konstantinovsky, E. A. Perets, E. C. Y. Yan, and S. Hammes-Schiffer, "Simulation of the chiral sum frequency generation response of supramolecular structures requires vibrational couplings," J. Phys. Chem. B 125(43), 12072-12081 (2021).
- ⁷J. Wang, X. Chen, M. L. Clarke, and Z. Chen, "Detection of chiral sum frequency generation vibrational spectra of proteins and peptides at interfaces in situ," Proc. Natl. Acad. Sci. U. S. A. 102(14), 4978-4983 (2005).
- ⁸G. Y. Stokes, J. M. Gibbs-Davis, F. C. Boman, B. R. Stepp, A. G. Condie, S. T. Nguyen, and F. M. Geiger, "Making 'sense' of DNA," J. Am. Chem. Soc. 129(24), 7492-7493 (2007).
- ⁹E. C. Y. Yan, L. Fu, Z. Wang, and W. Liu, "Biological macromolecules at interfaces probed by chiral vibrational sum frequency generation spectroscopy," Chem. Rev. 114(17), 8471-8498 (2014).
- $^{\bf 10} {\rm L.}$ Fu, J. Liu, and E. C. Y. Yan, "Chiral sum frequency generation spectroscopy for characterizing protein secondary structures at interfaces," J. Am. Chem. Sci 133(21), 8094-8097 (2011).
- ¹¹L. Fu, Z. Wang, and E. C. Y. Yan, "Chiral vibrational structures of proteins at interfaces probed by sum frequency generation spectroscopy," Int. J. Mol. Sci. **12**(12), 9404-9425 (2011).
- 12 A. J. Moad and G. J. Simpson, "A unified treatment of selection rules and symmetry relations for sum-frequency and second harmonic spectroscopies," J. Phys. Chem. B 108(11), 3548-3562 (2004).
- ¹³G. J. Simpson, "Molecular origins of the remarkable chiral sensitivity of secondorder nonlinear optics," ChemPhysChem 5(9), 1301-1310 (2004).
- ¹⁴B. M. Auer and J. L. Skinner, "Dynamical effects in line shapes for coupled chromophores: Time-averaging approximation," J. Chem. Phys. 127(10), 104105 (2007).
- ¹⁵Y. R. Shen, The Principles of Nonlinear Optics (Wiley, 2003).

- 16D. S. Walker and G. L. Richmond, "Understanding the effects of hydrogen bonding at the vapor-water interface: Vibrational sum frequency spectroscopy of H₂O/HOD/D₂O mixtures studied using molecular dynamics simulations," J. Phys. Chem. C 111(23), 8321-8330 (2007).
- ¹⁷Q. Du, R. Superfine, E. Freysz, and Y. R. Shen, "Vibrational spectroscopy of water at the vapor/water interface," Phys. Rev. Lett. 70(15), 2313 (1993).
- ¹⁸G. J. Simpson, Nonlinear Optical Polarization Analysis in Chemistry and Biology (Cambridge University Press, Cambridge, 2017).
- ¹⁹H.-F. Wang, L. Velarde, W. Gan, and L. Fu, "Quantitative sum-frequency generation vibrational spectroscopy of molecular surfaces and interfaces: Lineshape, polarization, and orientation," Annu. Rev. Phys. Chem. **66**(1), 189–216 (2015). ²⁰B. M. Auer and J. L. Skinner, "IR and Raman spectra of liquid water: Theory and
- interpretation," J. Chem. Phys. 128(22), 224511 (2008).
- ²¹D. Konstantinovsky, E. A. Perets, T. Santiago, K. Olesen, Z. Wang, A. V. Soudackov, E. C. Y. Yan, and S. Hammes-Schiffer, "Design of an electrostatic frequency map for the NH stretch of the protein backbone and application to chiral sum frequency generation spectroscopy," J. Phys. Chem. B 127(11), 2418-2429
- ²²W. F. DeGrado and J. D. Lear, "Induction of peptide conformation at apolar water interfaces. 1. A study with model peptides of defined hydrophobic periodicity," J. Am. Chem. Soc. **107**(25), 7684–7689 (1985).

 23 D. C. Phillips, R. L. York, O. Mermut, K. R. McCrea, R. S. Ward, and G. A.
- Somorjai, "Side chain, chain length, and sequence effects on amphiphilic peptide adsorption at hydrophobic and hydrophilic surfaces studied by sum-frequency generation vibrational spectroscopy and quartz crystal microbalance," J. Phys. Chem. C 111(1), 255-261 (2007).
- ²⁴R. L. York, W. K. Browne, P. L. Geissler, and G. A. Somorjai, "Peptides adsorbed on hydrophobic surfaces—A sum frequency generation vibrational spectroscopy and modeling study," Isr. J. Chem. 47(1), 51-58 (2007).
- ²⁵T. Weidner and D. G. Castner, "SFG analysis of surface bound proteins: A route towards structure determination," Phys. Chem. Chem. Phys. 15(30), 12516-12524
- ²⁶L. Fu, S.-L. Chen, and H.-F. Wang, "Validation of spectra and phase in sub-1 cm⁻¹ resolution sum-frequency generation vibrational spectroscopy through internal heterodyne phase-resolved measurement," J. Phys. Chem. B 120(8), 1579-1589 (2016).

- ²⁷J.-H. Choi, S. Hahn, and M. Cho, "Amide I IR, VCD, and 2d IR spectra of isotope-labeled α -helix in liquid water: Numerical simulation studies," Int. J. Quantum Chem. 104(5), 616-634 (2005).
- $^{\mathbf{28}}\mathrm{Z}.$ Ganim and A. Tokmakoff, "Spectral signatures of heterogeneous protein ensembles revealed by MD simulations of 2DIR spectra," Biophys. J. 91(7), 2636-2646 (2006).
- ²⁹S. Hahn, S. Ham, and M. Cho, "Simulation studies of amide I IR absorption and two-dimensional IR spectra of β hairpins in liquid water," J. Phys. Chem. B **109**(23), 11789-11801 (2005).
- 30 A. C. Belch and S. A. Rice, "The OH stretching spectrum of liquid water: A random network model interpretation," J. Chem. Phys. 78(8), 4817-4823
- $^{\bf 31}\,{\rm B.}$ M. Auer and J. L. Skinner, "Vibrational sum-frequency spectroscopy of the water liquid/vapor interface," J. Phys. Chem. B 113(13), 4125-4130 (2009).
- 32 J. R. Schmidt, S. A. Corcelli, and J. L. Skinner, "Ultrafast vibrational spectroscopy of water and aqueous N-methylacetamide: Comparison of different electronic structure/molecular dynamics approaches," J. Chem. Phys. 121, 8887
- 33 S. A. Corcelli and J. L. Skinner, "Infrared and Raman line shapes of dilute HOD in liquid H₂O and D₂O from 10 to 90 °C," J. Phys. Chem. A 109(28), 6154-6165
- ³⁴P. A. Pieniazek, C. J. Tainter, and J. L. Skinner, "Interpretation of the water surface vibrational sum-frequency spectrum," J. Chem. Phys. 135, 044701
- 35 T. la Cour Jansen and J. Knoester, "A transferable electrostatic map for solvation effects on amide I vibrations and its application to linear and two-dimensional spectroscopy," J. Chem. Phys. 124, 044502 (2006).
- ³⁶T. la Cour Jansen, A. G. Dijkstra, T. M. Watson, J. D. Hirst, and J. Knoester, "Modeling the amide I bands of small peptides," J. Chem. Phys. 125, 044312
- ³⁷S. A. Corcelli, C. P. Lawrence, and J. L. Skinner, "Combined electronic structure/molecular dynamics approach for ultrafast infrared spectroscopy of dilute HOD in liquid H₂O and D₂O," J. Chem. Phys. 120(17), 8107-8117
- ³⁸D. Konstantinovsky, E. C. Y. Yan, and S. Hammes-Schiffer, "Characterizing interfaces by Voronoi tessellation," J. Phys. Chem. Lett. 14(23), 5260-5266 (2023).